JGR Space Physics

RESEARCH ARTICLE

10.1029/2023JA031311

Key Points:

- Three-dimensional particle-in-cell simulation of magnetosonic (MS) wave excitation in a dipole magnetic field has been studied for the first time
- The linear growth rates of MS waves are almost equal in the radial and azimuthal directions
- A larger wave amplification is observed in the azimuthal direction since the waves can grow for a longer time in this direction

Supporting Information:

Supporting Information may be found in the online version of this article.

Correspondence to:

J. Sun and B. Zhang,
sunjicheng@pric.org.cn;
zhangbeichen@pric.org.cn

Citation:

Sun, J., Wang, X., Lu, Q., Zhang, B., Hu, Z., Liu, J., et al. (2023). Excitation and propagation of magnetosonic waves in the Earth's dipole magnetic field: 3D PIC simulation. *Journal of Geophysical Research: Space Physics*, *128*, e2023JA031311. https://doi.org/10.1029/2023JA031311

Received 21 MAR 2023
Accepted 15 AUG 2023

Excitation and Propagation of Magnetosonic Waves in the Earth's Dipole Magnetic Field: 3D PIC Simulation

Jicheng Sun[1], Xueyi Wang[2], Quanming Lu[3], Beichen Zhang[1], Zejun Hu[1], Jianjun Liu[1], Hongqiao Hu[1], and Huigen Yang[1]

[1]MNR Key Laboratory for Polar Science, Polar Research Institute of China, Shanghai, China, [2]Department of Physics, Auburn University, Auburn, AL, USA, [3]CAS Key Laboratory of Geospace Environment, Department of Geophysics and Planetary Science, University of Science and Technology of China, Hefei, China

Abstract Magnetosonic (MS) waves are common plasma waves in the Earth's magnetosphere. The self-consistent excitation of MS waves has been studied by 2D particle-in-cell simulations in the meridian and equatorial planes of a dipole magnetic field. However, the direction of wave propagation is artificially limited in the previous 2D simulations. Therefore, the 3D simulation of MS waves needs to be investigated. In this paper, we investigate the excitation and evolution of MS waves in the Earth's dipole magnetic field based on a 3D general curvilinear particle-in-cell simulation. We find that the MS waves are excited primarily within 3° of the equator when the thermal velocity of the ring distribution is much less than the ring velocity of the ring distribution. These waves propagate along both the radial and azimuthal directions nearly perpendicular to the background magnetic field. In the linear stage, the growth rates of MS waves are almost equal in the radial and azimuthal directions. Compared with the waves propagating along the radial direction, the waves propagating along the azimuthal direction can grow for a longer time, resulting in a larger wave amplification in this direction after saturation. The simulation results provide a valuable insight to understand the self-consistent evolution of MS waves in the Earth's dipole magnetic field, and the findings are useful for understanding the plasma wave-particle interaction in the Earth's radiation belts.

Plain Language Summary The Earth's magnetosphere is a natural plasma laboratory. Since the plasma in the magnetosphere is collisionless, electromagnetic waves are significant agents for the transport of energy and momentum among different particles. The MS waves are important electromagnetic waves in the magnetosphere, which have a frequency range from several Hertz to several hundred Hertz. Recently, these waves have been receiving an increasing interest due to their potential importance in accelerating radiation belt electrons and heating plasmaspheric ions. The 2D particle-in-cell simulations have been used to investigate MS waves in the meridian and equatorial planes of a dipole magnetic field. However, the direction of wave propagation is artificially limited in the previous 2D simulations. Thus, the 3D simulation of MS waves still needs to be studied. In this paper, we perform a 3D particle-in-cell simulation to investigate the excitation of the MS waves in a dipole magnetic field. A larger wave amplification is found in the azimuthal direction because they can grow for a longer time in this direction. Our results can contribute to the understanding of the spatial distribution of MS waves in the Earth's magnetosphere.

1. Introduction

Magnetosonic (MS) waves, also referred to as equatorial noise, are common electromagnetic waves in the Earth's magnetosphere (Russell et al., 1970; Santolík et al., 2002). These waves have a frequency range from several Hertz to several hundred Hertz, roughly between the local proton cyclotron frequency and the low hybrid frequency (e.g., Balikhin et al., 2015). The statistical study by Ma et al. (2013) indicated that strong MS waves have the root-mean-square amplitudes ~50 pT and an occurrence rate ~20% outside the plasmapause. Satellite observations and numerical simulations have revealed that the MS waves can be excited by the ring distribution protons with energy in the vicinity of 10 keV (Liu et al., 2011; Meredith et al., 2008; Perraut et al., 1982; Sun et al., 2016a, 2020a). Moreover, it was shown that the wave excitation can be modulated by the plasmaspheric density (Sun et al., 2021; Yuan et al., 2017). MS waves in the Earth's inner magnetosphere usually occur at several harmonics of the local proton cyclotron frequency (e.g., Balikhin et al., 2015). Recent observations also showed that MS waves sometimes exhibit the rising-tone (Boardsen et al., 2014; Fu et al., 2014) and continuous spectrum (Tsurutani et al., 2014). Subsequently, Sun et al. (2016a, 2020b) employed particle-in-cell (PIC) simulations to

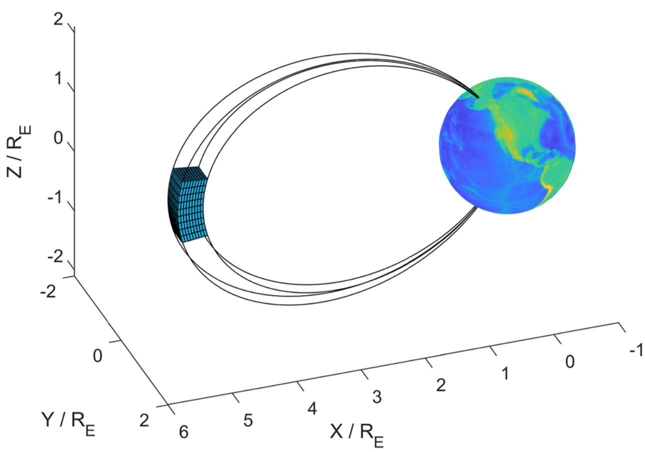

Figure 1. The simulation domain in Cartesian coordinates. The black lines represent the magnetic field lines.

reconstruct these phenomena. The simulation revealed that the strong wave intensity leads to the formation of the continuous MS wave spectrum, while the rising-tone MS waves can be attributed to the scattering of ring distribution protons.

MS waves have been receiving more attention recently because of their potential role in accelerating and scattering relativistic electrons in the radiation belts through Landau resonance (Horne et al., 2007), transit time effects (Bortnik & Thorne, 2010; Li et al., 2014), and bounce resonance (Chen et al., 2015; Tao & Li, 2016). According to Horne et al. (2007), the timescale of electron acceleration by MS waves through Landau resonance can be as short as 1 day, which is comparable to that of electron acceleration through cyclotron resonance with whistler-mode chorus (Horne et al., 2005). The quasi-linear theory further shows that the combined acceleration by chorus and MS waves can lead to the butterfly pitch angle distribution of relativistic electrons (Xiao et al., 2015). In addition to the interaction with radiation belt electrons, PIC simulations and satellite observations revealed that the MS waves could also heat cold ions in the density cavity of the plasmasphere (Sun et al., 2017, 2021; Yuan et al., 2018).

The propagation direction of MS waves is almost perpendicular to the background magnetic field, which means that MS waves can propagate along the radial and azimuthal directions (Su et al., 2017). Analysis of Van Allen Probes data by Boardsen et al. (2018) in a near-source event indicated a preference for azimuthal wave vector orientation. Then, Min et al. (2018) demonstrated the observation results using the 2D PIC simulation at the dipole magnetic equator. However, the wave normal angle is strictly limited to 90° in the 2D simulation. Therefore, the generation and propagation of MS waves in a 3D dipole magnetic field still need to be investigated. In this paper, using a 3D general curvilinear particle-in-cell (gc-PIC) simulation, we investigate the excitation and propagation of the MS waves in the Earth's dipole magnetic field for the first time. The structure of this paper is organized as follows. The simulation model and initial parameters are described in Section 2. Then, the simulation results are given in Section 3. Finally, the conclusions and discussion are presented in Section 4.

2. Simulation Model

In this paper, we use a 3D gc-PIC simulation to investigate the MS wave excitation in a dipole magnetic field. The grid used in the simulation is based on a modified dipole coordinate system (r,q,ϕ), in which r denotes L-shell, q varies along the dipole magnetic field, and ϕ is the magnetic longitude (Chen et al., 2018). The coordinate q is defined by the following equation:

$$12q^3 + q = \frac{L_0^2 \sin\lambda}{r^2}, \tag{1}$$

where L_0 is the center L-shell of the simulation domain, λ is the magnetic latitude, and $q = 0$ represents the magnetic equator. Figure 1 illustrates the computational domain of our study with reduced grid points in the Cartesian coordinates. The simulation domain consists of a $256 \times 64 \times 256$ grid of evenly distributed bins in the ranges [4.8, 5.2], [−0.1, 0.1], and [−2.3°, 2.3°] for (r,q,ϕ) directions, respectively. The value of $q = 0.1$ for the center r corresponds to $\lambda \approx 6.5°$.

For the initial condition, we choose the same three-component plasma as Chen et al. (2018): cold electrons and protons with a Maxwellian distribution, and hot protons with a ring distribution. For each species, there are on average 1,000 superparticles in each cell. In the following discussions, subscripts e, pc, and pr represent cold electrons, cold protons, and ring distribution protons, respectively. The difference between our initial conditions and Chen et al. (2018) is that the ring distribution protons are evenly distributed in the equatorial plane rather than placed locally. The following form is adopted as the distribution of ring protons at the equator,

$$f_r(v_\parallel, v_\perp) = \frac{n_{pr,eq}}{\pi^{3/2} v_{rt}^3 C} \exp\left(-\frac{(v_\perp - V_r)^2}{v_{rt}^2}\right) \exp\left(-\frac{v_\parallel^2}{v_{rt}^2}\right) \tag{2}$$

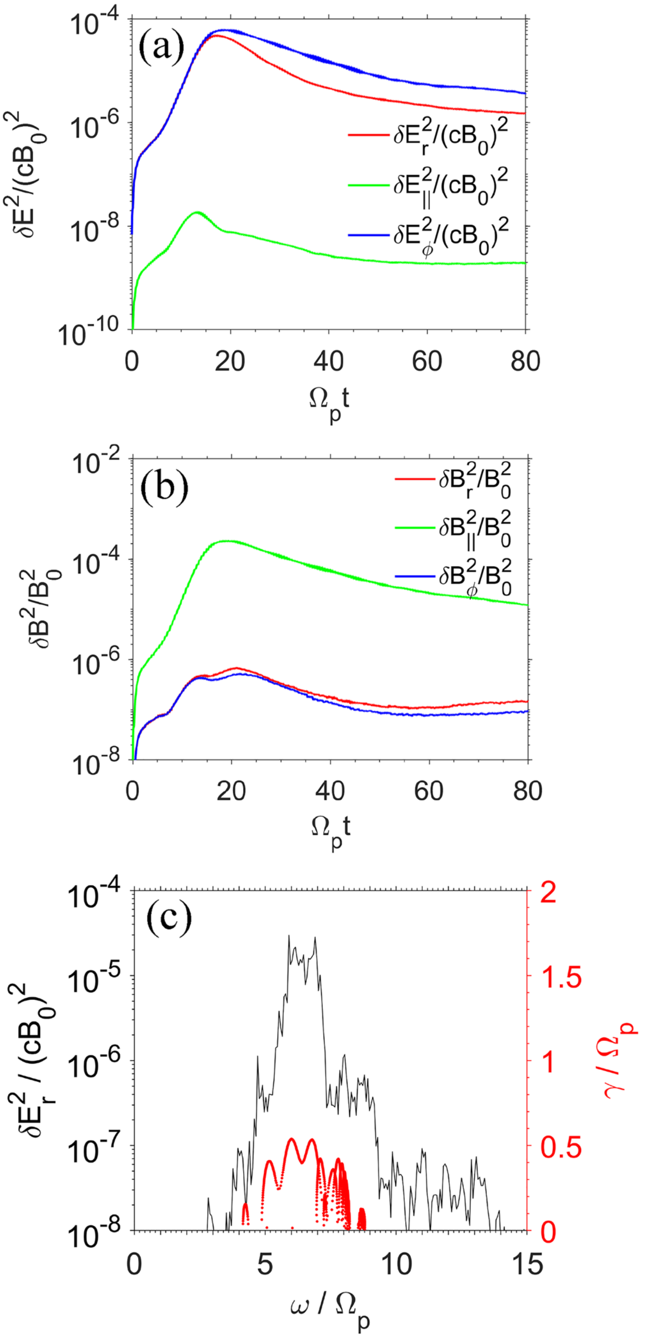

Figure 2. The time evolution of spatially averaged fluctuating (a) electric fields and (b) magnetic fields, and (c) The power spectrum density of fluctuating electric fields E_r/cB_0 at the position (L_0, 0,0) over the time interval from $\Omega_p t = 0$ to 80. The red dots in the figure represent normalized linear growth rate γ/Ω_p obtained from linear theory using the same parameters as the simulation.

$$C = \exp\left(-\left(\frac{V_r}{v_{rt}}\right)^2\right) + \sqrt{\pi}\frac{V_r}{v_{rt}}\mathrm{erfc}\left(-\frac{V_r}{v_{rt}}\right), \tag{3}$$

where $v_{\|}$ and $v_{\perp}$ are velocities parallel and perpendicular to the background magnetic field, v_{rt} is the thermal speed of the ring distribution, V_r is the proton ring velocity, $n_{pr,eq}$ is the number density of ring protons at the equator, and erfc is the complementary error function. The distribution function of the off-equator ring protons can be obtained using the Liouville's theorem.

In the simulation, the magnetic field is normalized by the dipole magnetic field B_0 at the center point of the simulation domain $(r,q,\phi) = (L_0,0,0)$. The time and space are normalized to the inverse of electron gyrofrequency Ω_e and the electron gyroradius ρ_e at that location, respectively. The ring proton number density at the equator is $n_{pr,eq} = 0.05n_{e0}$, where n_{e0} is the electron number density at $(L_0,0,0)$. For reducing computational cost, the mass ratio of proton to electron and the speed of light are reduced to be $m_p/m_e = 100$ and $c = 20V_A$, where $V_A = \mathrm{B}_0/\sqrt{\mu_0 n_{e0} m_p}$ is the Alfven speed at the position (L_0, 0, 0). For the chosen value of the mass ratio, the proton gyrofrequency is $\Omega_p = 0.01\Omega_e$. In this study, the ring distribution is initialized as $V_r = V_A$ (the Alfven speed at the position (L_0, 0, 0)) and $v_{rt} = 0.01V_A$. Thus, there are the same ring distribution at different L-shell. The time step Δt is set as $\Omega_e \Delta t = 0.05$. When translated to the physical setup, the central magnetic field line corresponds to $L_0 = 5$, $B_0 = 248$ nT, and $n_{e0} = 10\ \mathrm{cm}^{-3}$. The cold electron and proton temperature are 1 eV. These simulation parameters are the typical values of the plasma outside the plasmasphere near the equator. The absorbing boundary conditions are assumed for electromagnetic fields and reflecting boundary conditions are used for particles.

3. Simulation Results

With the 3D gc-PIC simulation model and the initial setup described above, we investigate the excitation and evolution of MS waves in the Earth's magnetosphere. Figures 2a and 2b show the time evolution of spatially averaged fluctuating electromagnetic fields for the simulation. It can be seen that the waves are excited at first and then undergo a linear growth stage before reaching saturation around $\Omega_p t = 20$. The dominant wave power is found in δE_r, δE_ϕ, and $\delta B_{\|}$. This indicates that the waves possess a compressional magnetic field, which is consistent with the polarization of MS waves predicted by the linear theory (Gary et al., 2010). In order to confirm that the excited fluctuations are MS waves, we compared the simulation results with the linear theory. It is noted that we use the same parameters in the linear theory model as the simulation at the position (L_0, 0, 0). Figure 2c displays the power spectrum of radial fluctuating electric field δE_r at the position (L_0, 0, 0) over the time interval from $\Omega_p t = 0$ to 80. Red dots signify the normalized linear growth rate with the wave normal angle $\theta = 90°$ calculated by the linear theory. As we can see, the frequency peaks of the wave spectrum at $\omega/\Omega_p = 6$ and 7 agree well with that of the positive growth rate predicted by the linear theory. Moreover, the magnitude of the growth rate ($\sim 0.3\Omega_p$) estimated from the temporal profile of δE_r is also comparable to the linear growth rate ($\sim 0.5\Omega_p$) from linear theory. The peaks at frequencies greater than $10\Omega_p$ obtained from the simulation, inconsistent with the linear theory, may be due to the waves near perpendicular propagation ($\theta \neq 90°$) (Chen, 2015). Based on the above analysis, we confirm that the simulated fluctuating electromagnetic fields indeed manifest as MS waves generated by the ring distribution proton. Furthermore, we compare the simulation results with Min et al. (2018). The 2D PIC simulation at the dipole magnetic equator is used in Min et al. (2018), in which the wave normal

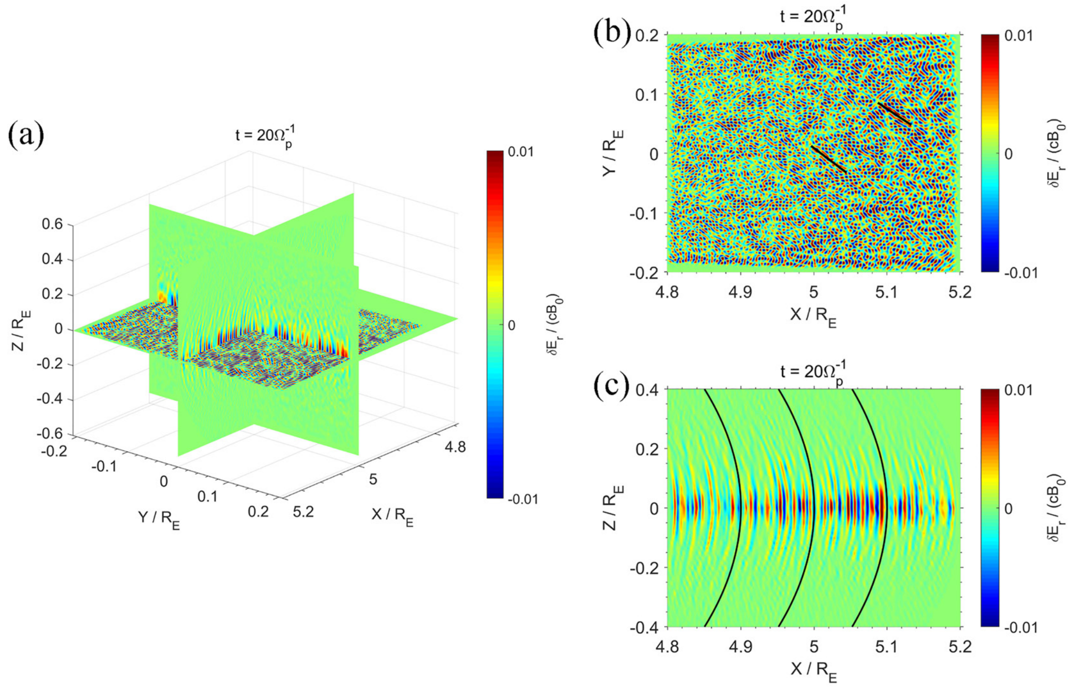

Figure 3. The spatial distribution of the fluctuating electric fields δE_r in (a) the 3D Cartesian coordinates, (b) the equatorial plane, and (c) the meridian plane at $\Omega_p t = 20$. The black lines in (b) mark the sloped wave fronts in the equatorial plane, while the black curves in (c) represent the magnetic field lines in the meridian plane.

angle of MS waves is strictly limited to 90°. Thus, the fluctuating magnetic fields have no perpendicular components and only parallel components, while the fluctuating electric fields have only perpendicular components and no parallel components. In contrast, our 3D PIC simulation allows the MS wave normal angle to deviate from 90°. This results in the presence of perpendicular fluctuating magnetic fields and parallel fluctuating electric fields in our simulation, which is more consistent with the properties of magnetosonic waves in the real magnetosphere.

Figure 3 displays the spatial distribution of the fluctuating electric fields δE_r at $\Omega_p t = 20$ in the 3D Cartesian coordinates (Figure 3a), the equatorial plane (Figure 3b), and the meridian plane (Figure 3c). The black lines in Figure 3b mark the sloped wave fronts in the equatorial plane, while the black curves in Figure 3c represent the magnetic field lines in the meridian plane. From the temporal evolution of fluctuating electromagnetic fields (Figure 2a), the MS waves just reach the saturation stage at this time. We can see from Figure 3a that the MS waves are excited primarily within 3° of the equator. In the meridian plane (Figure 3c), it can be seen more clearly that the wave intensity is concentrated near the equator. In addition, nearly constant wave fronts are along the magnetic field lines, suggesting that the excited MS waves propagate almost perpendicular to the background magnetic field. From Figure 3b, the wave fronts are sloped in the *X*-*Y* plane, which indicates that the MS wave propagation (normal to wave fronts) is in both the radial and azimuthal directions. We also analyze the fluctuating electric fields in the azimuthal direction δE_ϕ (not shown), and their spatial distribution is similar to that of δE_r at this time.

To determine the propagation direction of MS waves, we analyze the fluctuating magnetic field $\delta B_\parallel$ at the magnetic equator at different time. Figure 4 shows snapshots of the compressional component of the fluctuating magnetic field $\delta B_\parallel$ at the magnetic equator at $\Omega_p t = 15$ and 30, and the corresponding wave number spectrum. In order to see the waveforms of the MS waves more clearly, a zoom-in view of the equatorial plane in the simulation is shown ($4.9R_E \le r \le 5.1R_E$ and $-1° \le \phi \le 1°$). The value of $\phi = 1°$ for the center r corresponds to about $0.09R_E$. Thus, the vertical and horizontal length ratio is realistic in the snapshots. At the linear growth stage ($\Omega_p t = 15$), both the snapshot of $\delta B_\parallel$ and the wave number spectrum show that the MS waves propagate along both the radial and azimuthal directions perpendicular to the background magnetic field. We define $\varphi = \arctan(|k_\phi/k_r|)$ to measure whether the MS waves propagate along the radial or azimuthal direction. From the wave number spectrum, we can see that the MS wave modes with large amplitude are mainly concen-

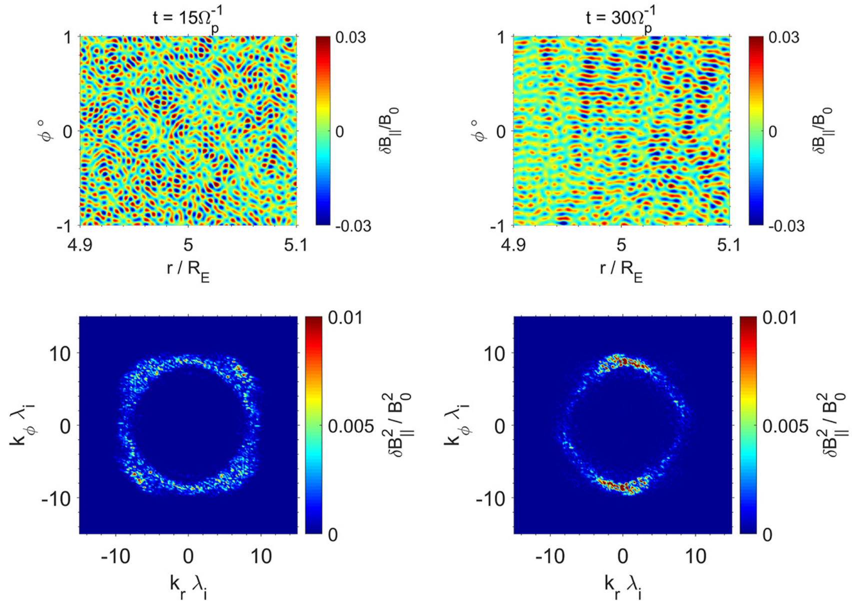

Figure 4. The snapshots of $\delta B_\parallel$ at $\Omega_p t = 15$ and 30, and the corresponding wave number spectrum.

trated around $\varphi = 45°$ at $\Omega_p t = 15$, which means that the propagation of MS waves in the equatorial plane has no preference at this time between the radial and azimuthal directions. At $\Omega_p t = 30$, it can be seen from the snapshot that the MS waves mainly propagate along the azimuthal direction (see also the Movie S1). From the wave number spectrum at $\Omega_p t = 30$, we can find that the dominant wave modes are mainly distributed in $8\lambda_i^{-1} < |k_\phi| < 10\lambda_i^{-1}$ and $0\lambda_i^{-1} < |k_r| < 4\lambda_i^{-1}$, where $\lambda_i = V_A/\Omega_p$ is the proton inertial length. The $|k_\phi|$ is much larger than $|k_r|$, which also indicates the MS waves mainly propagate along the azimuthal direction (see also the Movie S2).

Figure 5 displays the time evolution of compressional magnetic field amplitudes for quasi-radial ($0° \leq \varphi < 45°$) and quasi-azimuthal ($45° < \varphi \leq 90°$) propagating MS wave modes. We perform a 2D Fourier transforming of $\delta B_\parallel$ of MS waves at the magnetic equator at each time. From Figure 4, we can find that the wave number of simulated MS waves is mainly distributed in $8\lambda_i^{-1} < |k| < 10\lambda_i^{-1}$. Consequently, we select the wave modes of $|k|$ between $8\lambda_i^{-1}$ and $10\lambda_i^{-1}$ to calculate the power of quasi-radial and quasi-azimuthal MS wave modes. The wave amplitudes for quasi-radial and quasi-azimuthal MS waves can be examined by averaging the power of these wave modes for $0° \leq \varphi < 45°$ and $45° < \varphi \leq 90°$. Before $\Omega_p t = 15$, one can see that the amplitudes of quasi-radial and quasi-azimuthal MS wave modes are almost equal all the time. This indicates that the growth rates of these waves are almost equal in the radial and azimuthal directions. At about $\Omega_p t = 15$, the quasi-radial MS waves are saturated, while the quasi-azimuthal MS waves can grow until about $\Omega_p t = 20$. This extended growth duration for azimuthal waves results in their dominance during saturation. The power of quasi-azimuthal MS waves is about 5–15 times larger than those of quasi-radial MS at saturation. Also, the propagation direction of the waves can be roughly determined by the intensity ratio between δE_r and δE_ϕ, since the electric field fluctuations of MS waves are predominantly electrostatic. It can be seen from Figure 2a that the intensities of δE_r and δE_ϕ are almost equal until δE_r saturates at about $\Omega_p t = 15$, while δE_ϕ can grow until about $\Omega_p t = 20$. This also indicates that the MS waves propagating along the azimuthal direction can grow for a longer time. In the azimuthal direction, the MS waves can continuously grow along the magnetic field contour since there is a constant proton ring distribution in our simulation. In contrast, because of the radial variation of magnetic field magnitude, the MS waves will grow for a shorter time along the radial direction.

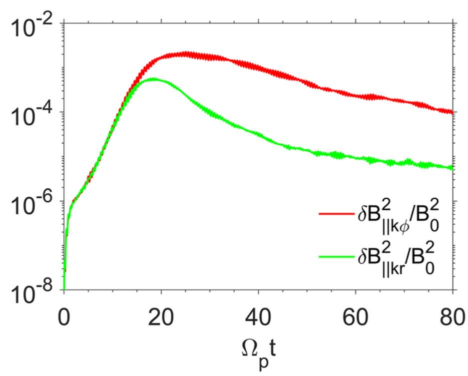

Figure 5. The time evolution of compressional magnetic field amplitudes for quasi-radial ($0° \leq \varphi < 45°$) and quasi-azimuthal ($45° < \varphi \leq 90°$) MS wave modes ($8\lambda_i^{-1} < |k| < 10\lambda_i^{-1}$).

4. Conclusions and Discussion

In this paper, by performing a 3D gc-PIC simulation, we have examined the generation and evolution of MS waves in the Earth's dipole magnetic field. The simulation model consists of three plasma components: ring distribution protons as free energy, background cold electrons and protons. We found that the MS waves are initially excited near the equator and propagate nearly perpendicular to the background magnetic field. These waves are primarily confined within 3° of the equator. The linear growth rates of these waves are almost equal in the radial and azimuthal directions. Compared with the waves propagating along the radial direction, the MS waves propagating along the azimuthal direction can grow for a longer time, resulting in the wave amplification mainly during the azimuthal propagation.

Boardsen et al. (2018) analyzed a near-source MS wave event and found that the wave vector is preferentially in the azimuthal direction. Then, Min et al. (2018) demonstrated this observation result using the 2D PIC simulation at the dipole magnetic equator. It is worth comparing the differences and similarities in the initial setup and simulation results between our simulation and theirs. In Min et al. (2018), the 2D PIC simulation at the dipole magnetic equator was used to study the MS wave generation and evolution, in which the wave normal angle of MS waves is limited to 90°. Consequently, there are only the parallel fluctuating magnetic fields and the perpendicular fluctuating electric fields in their simulation. However, our 3D PIC simulation allows the wave normal angle of MS waves to deviate from 90°, which results in the presence of the perpendicular fluctuating magnetic fields and the parallel fluctuating electric fields in our simulation. In terms of the simulation parameters, both simulation assume a reduced mass ratio and a smaller light speed to save the computational resources. For the saturation time of MS waves, compared with the results of Min et al. (2018), the saturation of excited MS waves in the present simulation is faster. The reason is that the free energy chosen by Min et al. (2018) was the shell distribution proton, while we use the ring distribution proton. The ring distribution releases free energy faster. For the generation and evolution of MS waves, our conclusion that the wave amplification occurs dominantly during the azimuthal propagation is consistent with Min et al. (2018). Moreover, our simulation results further confirm that the wave amplification dominated by the azimuthal direction is due to the longer growth time in that direction. In the linear stage, the linear growth rates of MS waves are almost equal in the radial and azimuthal directions.

In the simulation, reflecting boundary conditions are used for particles in both the radial and azimuthal directions. The identical boundary conditions allow us to ensure that the boundary conditions are not the source of the MS wave amplification dominated by the azimuthal direction. We also examined the effect of boundary conditions on the simulation results. If the periodic boundary conditions are adopted for particles in the radial direction, the saturated amplitude of the waves propagating along the radial direction will be larger than the results using the reflecting boundary condition. However, the conclusion that MS waves propagate mainly along the azimuthal direction for the saturated stage remains unaffected. Moreover, the off-equator MS wave propagation is also diagnosed. Since the MS waves excited in this simulation are basically near the equatorial plane (less than 3°), the results of the off-equator MS wave propagation are very close to that of MS waves in the equatorial plane.

Limited by the computational resources, a reduced mass ratio ($m_p/m_e = 100$) and a smaller light speed ($c = 20V_A$) are chosen in our simulations. This will lead to a reduced lower hybrid frequency, and a change in the MS wave spectrum (Sun et al., 2016b). However, this does not affect the main conclusions of this paper. The growth rates of MS wave excitation in the radial and azimuthal directions are almost equal in the Earth's dipole magnetic field, and the saturated amplitude is dominated by the azimuthal direction because these waves can grow longer in that direction. Since the saturated amplitude of the MS waves is closely related to the growth time, the excitation and propagation characteristics of MS waves with different scale ratios of the source region (the radial and azimuthal spatial scale ratio) are worth to further study. In addition to the near-equator MS waves, the observations have shown that MS waves can also be generated at mid-latitudes (Wu et al., 2021, 2022). We have investigated the excitation and evolution of near-equator MS waves in this paper. The simulation of the MS waves at mid-latitudes will be studied in the future.

Data Availability Statement

The data set for this research is available in this in-text data citation reference: Sun (2022).

Acknowledgments

This work was supported by the National Natural Science Foundation of China (42204169, 41831072, and 42130210), and Shanghai Science and Technology Innovation Action Plan (No. 21DZ1206100). J. S. was sponsored by Shanghai Pujiang Program (No. 21PJD078).

References

Balikhin, M. A., Shprits, Y. Y., Walker, S. N., Chen, L., Cornilleau-Wehrlin, N., Dandouras, I., et al. (2015). Observations of discrete harmonics emerging from equatorial noise. *Nature Communications*, *6*(1), 7703. https://doi.org/10.1038/ncomms8703

Boardsen, S. A., Hospodarsky, G. B., Kletzing, C. A., Pfaff, R. F., Kurth, W. S., Wygant, J. R., & MacDonald, E. A. (2014). Van Allen probe observations of periodic rising frequencies of the fast magnetosonic mode. *Geophysical Research Letters*, *41*(23), 8161–8168. https://doi.org/10.1002/2014GL062020

Boardsen, S. A., Hospodarsky, G. B., Min, K., Averkamp, T. F., Bounds, S. R., Kletzing, C. A., & Pfaff, R. F. (2018). Determining the wave vector direction of equatorial fast magnetosonic waves. *Geophysical Research Letters*, *45*(16), 7951–7959. https://doi.org/10.1029/2018GL078695

Bortnik, J., & Thorne, R. M. (2010). Transit time scattering of energetic electrons due to equatorially confined magnetosonic waves. *Journal of Geophysical Research*, *115*(A7), A07213. https://doi.org/10.1029/2010JA015283

Chen, L. (2015). Wave normal angle and frequency characteristics of magnetosonic wave linear instability. *Geophysical Research Letters*, *42*(12), 4709–4715. https://doi.org/10.1002/2015GL064237

Chen, L., Maldonado, A., Bortnik, J., Thorne, R. M., Li, J., Dai, L., & Zhan, X. (2015). Nonlinear bounce resonances between magnetosonic waves and equatorially mirroring electrons. *Journal of Geophysical Research: Space Physics*, *120*(8), 6514–6527. https://doi.org/10.1002/2015JA021174

Chen, L., Sun, J., Lu, Q., Wang, X., Gao, X., Wang, D., & Wang, S. (2018). Two-dimensional particle-in-cell simulation of magnetosonic wave excitation in a dipole magnetic field. *Geophysical Research Letters*, *45*(17), 8712–8720. https://doi.org/10.1029/2018GL079067

Fu, H. S., Cao, J. B., Zhima, Z., Khotyaintsev, Y. V., Angelopoulos, V., Santolik, O., et al. (2014). First observation of rising-tone magnetosonic waves. *Geophysical Research Letters*, *41*(21), 7419–7426. https://doi.org/10.1002/2014GL061867

Gary, S. P., Liu, K., Winske, D., & Denton, R. E. (2010). Ion Bernstein instability in the terrestrial magnetosphere: Linear dispersion theory. *Journal of Geophysical Research*, *115*(A12), A12209. https://doi.org/10.1029/2010JA015965

Horne, R. B., Thorne, R. M., Glauert, S. A., Albert, J. M., Meredith, N. P., & Anderson, R. R. (2005). Timescale for radiation belt electron acceleration by whistler mode chorus waves. *Journal of Geophysical Research*, *110*(A3), A03225. https://doi.org/10.1029/2004JA010811

Horne, R. B., Thorne, R. M., Glauert, S. A., Meredith, N. P., Pokhotelov, D., & Santolik, O. (2007). Electron acceleration in the Van Allen radiation belts by fast magnetosonic waves. *Geophysical Research Letters*, *34*(17), L17107. https://doi.org/10.1029/2007GL030267

Li, J., Ni, B., Xie, L., Pu, Z., Bortnik, J., Thorne, R. M., et al. (2014). Interactions between magnetosonic waves and radiation belt electrons: Comparisons of quasi-linear calculations with test particle simulations. *Geophysical Research Letters*, *41*(14), 4828–4834. https://doi.org/10.1002/2014GL060461

Liu, K. J., Gary, S. P., & Winske, D. (2011). Excitation of magnetosonic waves in the terrestrial magnetosphere: Particle-in-cell simulations. *Journal of Geophysical Research*, *116*(A7), A07212. https://doi.org/10.1029/2010JA016372

Ma, Q. L., Li, W., Thorne, R. M., & Angelopoulos, V. (2013). Global distribution of equatorial magnetosonic waves observed by THEMIS. *Geophysical Research Letters*, *40*(10), 1895–1901. https://doi.org/10.1002/grl.50434

Meredith, N. P., Horne, R. B., & Anderson, R. R. (2008). Survey of magnetosonic waves and proton ring distributions in the Earth's inner magnetosphere. *Journal of Geophysical Research*, *113*(A6), A06213. https://doi.org/10.1029/2007JA012975

Min, K., Boardsen, S. A., Denton, R. E., & Liu, K. (2018). Equatorial evolution of the fast magnetosonic mode in the source region: Observation-simulation comparison of the preferential propagation direction. *Journal of Geophysical Research: Space Physics*, *123*(11), 9532–9544. https://doi.org/10.1029/2018JA026037

Perraut, S., Roux, A., Robert, P., Gendrin, R., Sauvaud, J., Bosqued, J., et al. (1982). A systematic study of ULF waves above F_{H+} from GEOS 1 and 2 measurements and their relationships with proton ring distributions. *Journal of Geophysical Research*, *87*(A8), 6219–6236. https://doi.org/10.1029/JA087iA08p06219

Russell, C. T., Holzer, R. E., & Smith, E. J. (1970). OGO 3 observations of ELF noise in the magnetosphere: 2. The nature of the equatorial noise. *Journal of Geophysical Research*, *75*(4), 755–768. https://doi.org/10.1029/JA075i004p00755

Santolik, O., Pickett, J. S., Gurnett, D. A., Maksimovic, M., & Cornilleau-Wehrlin, N. (2002). Spatiotemporal variability and propagation of equatorial noise observed by Cluster. *Journal of Geophysical Research*, *107*(A12), 1495. https://doi.org/10.1029/2001JA009159

Su, Z., Wang, G., Liu, N., Zheng, H., Wang, Y., & Wang, S. (2017). Direct observation of generation and propagation of magnetosonic waves following substorm injection. *Geophysical Research Letters*, *44*(15), 7587–7597. https://doi.org/10.1002/2017GL074362

Sun, J. (2022). Data for 3D PIC simulation of MS waves [Dataset]. Zenodo. https://doi.org/10.5281/zenodo.7267104

Sun, J., Chen, L., & Wang, X. (2020a). Wave normal angle distribution of magnetosonic waves in the Earth's magnetosphere: 2D PIC simulation. *Journal of Geophysical Research: Space Physics*, *125*(5), e2020JA028012. https://doi.org/10.1029/2020JA028012

Sun, J., Chen, L., Wang, X., Boardsen, S., Lin, Y., & Xia, Z. (2020b). Particle-in-cell simulation of rising-tone magnetosonic waves. *Geophysical Research Letters*, *47*(18), e2020GL089671. https://doi.org/10.1029/2020GL089671

Sun, J., Gao, X., Chen, L., Lu, Q., Tao, X., & Wang, S. (2016b). A parametric study for the generation of ion Bernstein modes from a discrete spectrum to a continuous one in the inner magnetosphere. I. Linear theory. *Physics of Plasmas*, *23*(2), 022901. https://doi.org/10.1063/1.4941283

Sun, J., Gao, X., Lu Q., Chen, L., Liu, X., Wang, X., et al. (2017). Spectral properties and associated plasma energization by magnetosonic waves in the Earth's magnetosphere: Particle-in-cell simulations. *Journal of Geophysical Research: Space Physics*, *122*(5), 5377–5390. https://doi.org/10.1002/2017JA024027

Sun, J., Gao, X., Lu, Q., Chen, L., Tao, X., & Wang, S. (2016a). A parametric study for the generation of ion Bernstein modes from a discrete spectrum to a continuous one in the inner magnetosphere. II. Particle-in-cell simulations. *Physics of Plasmas*, *23*(2), 022902. https://doi.org/10.1063/1.4941284

Sun, J., Lu, Q., Wang, X., Liu, X., Gao, X., & Yang, H. (2021). Modulation of magnetosonic waves by background plasma density in a dipole magnetic field: 2-D PIC simulation. *Journal of Geophysical Research: Space Physics*, *126*(11), e2021JA029729. https://doi.org/10.1029/2021JA029729

Tao, X., & Li, X. (2016). Theoretical bounce resonance diffusion coefficient for waves generated near the equatorial plane. *Geophysical Research Letters*, *43*(14), 7389–7397. https://doi.org/10.1002/2016GL070139

Tsurutani, B. T., Falkowski, B. J., Pickett, J. S., Verkhoglyadova, O. P., Santolik, O., & Lakhina, G. S. (2014). Extremely intense ELF magnetosonic waves: A survey of polar observations. *Journal of Geophysical Research: Space Physics*, *119*(2), 964–977. https://doi.org/10.1002/2013JA019284

Wu, Z., Su, Z., He, Z., Zheng, H., & Wang, Y. (2022). Magnetosonic waves above the lower hybrid frequency in cyclotron resonance with the Van Allen radiation belt electrons. *Geophysical Research Letters*, *49*(23), e2022GL100971. https://doi.org/10.1029/2022GL100971

Wu, Z., Su, Z., Liu, N., Gao, Z., Zheng, H., Wang, Y., & Wang, S. (2021). Off-equatorial source of magnetosonic waves extending above the lower hybrid resonance frequency in the inner magnetosphere. *Geophysical Research Letters*, *48*(6), e2020GL091830. https://doi.org/10.1029/2020GL091830

Xiao, F. L., Yang, C., Su, Z. P., Zhou, Q. H., He, Z. G., He, Y. H., et al. (2015). Wave-driven butterfly distribution of Van Allen belt relativistic electrons. *Nature Communications*, *6*(1), 8590. https://doi.org/10.1038/ncomms9590

Yuan, Z., Yu, X., Huang, S., Qiao, Z., Yao, F., & Funsten, H. O. (2018). Cold ion heating by magnetosonic waves in a density cavity of the plasmasphere. *Journal of Geophysical Research: Space Physics*, *123*(2), 1242–1250. https://doi.org/10.1002/2017JA024919

Yuan, Z., Yu, X., Huang, S., Wang, D., & Funsten, H. O. (2017). In situ observations of magnetosonic waves modulated by background plasma density. *Geophysical Research Letters*, *44*(15), 7628–7633. https://doi.org/10.1002/2017GL074681